https://doi.org/10.3311/PPtr.37240

Periodica Polytechnica Transportation Engineering, 53(1), pp. 77–86, 2025

Aerodynamic Study of Different Types of Wingtip Devices

Tamás Pálfi[1*], Péter Ficzere[1]

[1] Department of Railway Vehicles and Vehicle System Analysis, Faculty of Transportation Engineering and Vehicle Engineering, Budapest University of Technology and Economics, Műegyetem rkp. 3., H-1111 Budapest, Hungary
[*] Corresponding author, e-mail: palfi.tamas@edu.bme.hu

Received: 30 April 2024, Accepted: 05 September 2024, Published online: 13 September 2024

Abstract

The economic system of the 21st century requires technological solutions that ensure economical and sustainable passenger and freight transport, also by air. To this end, aircraft manufacturers are constantly working to make their aircraft as economical as possible.
The aim of the research is to examine the effectiveness of the CFD simulation programs by conducting wind tunnel tests. This research also studies different types of wingtip devices then compares the results to determine the most effective one in terms of aerodynamical drag reduction. In the course of the research, we test wingtip devices of various designs in a self-built wind tunnel, and then compare the measured data with the results of the computer simulation.

Keywords

wingtip device, induced drag, wingtip vortex, CFD simulation, wind tunnel

1 Introduction

During the past century, the aviation industry developed rapidly (Hallion, 2021), from the very first airplanes made of wood and canvas to modern airplanes made of composite materials weighing hundreds of tons. The economic system of the 21st century requires technological solutions that ensure economically sustainable (Timmons and Terwel, 2022) passenger and freight transport. In the last few decades, the aircraft industry has begun to develop rapidly, more and more innovations are constantly appearing on the market, but the development is far from being over, there are still many areas where development opportunities can be found. In this study, we examine one of these areas and find out its potential.

1.1 Basic aerodynamics

The forces affecting an airplane's wing are illustrated in Fig. 1, where F_y is the lift force, F_x is the drag force, F_p is the thrust, G is the weight of the aircraft, v is the flow velocity, and α is the angle of incidence.

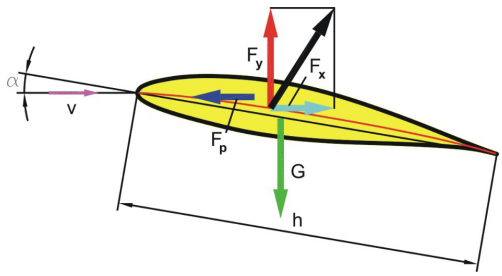

Fig. 1 Forces on a wing

1.2 Lift force

Examining the cross section of an airplane's wing, it can be observed that their contour has a greater curve on the upper section than on the lower section. This results in the air flowing on a longer path on the upper part than on the lower part (Restás, 2013). Bernoulli's law can be used to determine that the speed difference between the lower and upper surface of the wing of the airplane results in air pressure difference (Espinoza-Fraire et al., 2023) (Fig. 2).

1.3 Resistant forces

The force arising on bodies placed into the flow of a mass – parallel to the flow direction – is called resistance.

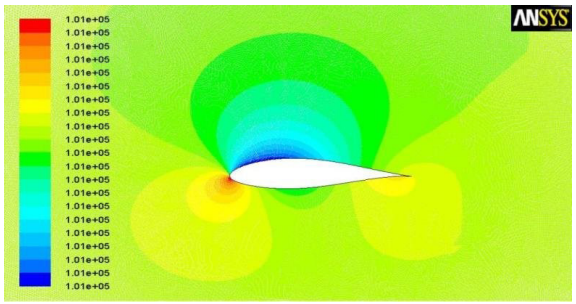

Fig. 2 Air pressure around the wing

Cite this article as: Pálfi, T., Ficzere, P. (2025) "Aerodynamic Study of Different Types of Wingtip Devices", Periodica Polytechnica Transportation Engineering, 53(1), pp. 77–86. https://doi.org/10.3311/PPtr.37240

The total resistance force on a wing of an airplane has two major components: induced drag and parasitic drag (Gudmundsson, 2022).

The air pressure difference illustrated in Fig. 2 also has a negative effect: the mass of air tries to flow inward on the upper part of the wing due to the low pressure in the area, while the mass of air under the wing with higher air pressure results in an outward flow. These processes cause a spectacular phenomenon at the wingtips (Fig. 3), because the air flowing outward from the lower part of the wing leaves the lower part of the wing at the wingtip, while it starts to flow inward in its upper part resulting in the so-called induced drag.

The updraft at the wingtip turns into the so-called wingtip vortex (Schörder et al., 2022) behind the wing – this is illustrated in Fig. 4 – which, on the one hand, results in a resistance force on the aircraft and, on the other hand, it can be dangerous for other aircraft flying into the vortex.

If the sizes of wingtip vortex can be reduced, the total air resistance will also be reduced, therefore achieving more economical operation and reduced CO_2 emissions (David, 2024). In this study, we examine the possibilities of reducing the induced drag.

1.4 Wingtip devices

In order to reduce the induced drag, aircraft manufacturers use the so-called wingtip devices. With the help of Fig. 5, it is easy to compare the magnitude of the vortices generated on the wingtips equipped with wingtip devices and those without wingtip devices.

Wingtip devices can be very diverse in their size and shape, but the primary purpose of all of them is to reduce the air resistance of the aircraft.

The first wingtip device was introduced in civil aviation as a result of the increase in oil prices in 1973 (Sy et al., 2020). Since then, aircraft manufacturers have been constantly working on designing better and better wingtip devices so their aircraft can save more fuel. Currently, by using the best winglets on an aircraft (Fig. 6) can result in 5–7% less fuel consumption, but this can be further improved, so the possibility still exists for engineers to design an even better wingtip device.

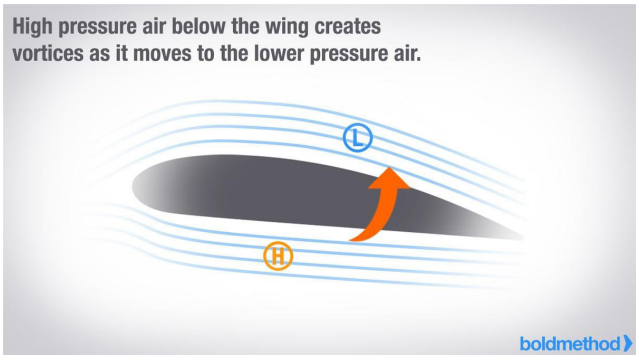

Fig. 3 Pressure difference on the wing

2 Methodology

2.1 Wind tunnel examinations

During the research, we would like to examine the behavior and efficiency of wingtips with different designs. To this end, wind tunnel tests are conducted for the flow studies, during which the updrafts created at the wingtips and the resulting vortices are studied.

2.1.1 Structure of the wind tunnel

The wind tunnel is a device designed for creating a controlled flow of a given medium (for example, air). It has

Fig. 4 Vortex behind the wingtip

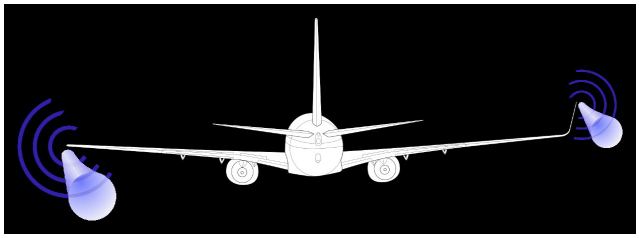

Fig. 5 Vortices on different types of wingtip

Fig. 6 Wingtip of Airbus A350

an examination space suitable for performing aeronautical tests and simulations.

A self-built wind tunnel is used for the tests, the dimensions of which are shown in Fig. 7.

The mentioned self-built wind tunnel (Fig. 8) is an open return wind tunnel, because the medium is not directly led back to the entrance. The ventilators ensuring the air flow are located on the exit side. On the inlet side, the parallel flow is ensured by 2,500 plastic straws. The examinations can be carried out in the experimental space between the straws and the ventilators, where the spectacular flow phenomenon can be easily observed due to the walls made of transparent plexiglas.

2.1.2 Producing models with additive manufacturing

Due to the complex geometry of the wings, the models for wind tunnel tests can be produced most efficiently using additive manufacturing, because in this way practically any model can be produced relatively quickly and on a low budget (Aghakhani and Takács, 2023).

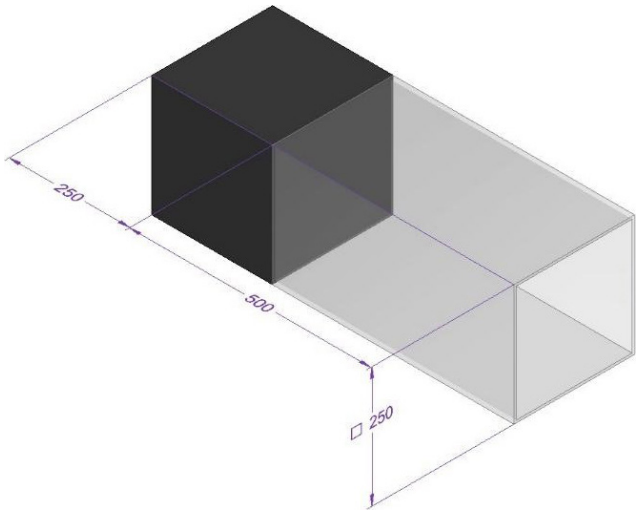

Fig. 7 The sizes of the wind tunnel

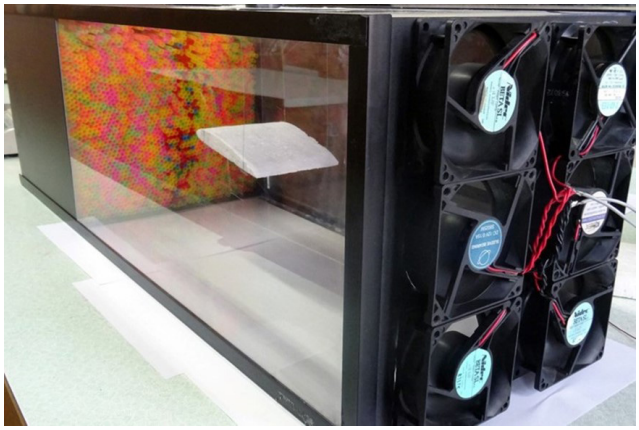

Fig. 8 Self-built wind tunnel

In order for the model to be easily examined in the wind tunnel, its geometric characteristics and dimensions were created using the design program Solid Edge, and then produced with the Zortrax M200 3D printer, which uses ABS material for printing.

Before starting the print job, it is necessary to choose the printing parameters (Kónya and Ficzere, 2024) regarding to the model being optimal for wind tunnel aerodynamic tests and simulations (Dul et al., 2022). Therefore, it is worth setting the printing layer thickness as thin as possible. Although this setting increases the production time, we get a significantly better surface roughness, thereby improving the accuracy of the simulation (Dömötör, 2023). The sketch of the model, sliced and with supports, can be seen in Fig. 9.

The models with different topologies can be mounted and adjusted to the desired position in the wind tunnel using a universal support, also produced by additive manufacturing. The support is attached to the wall of the wind tunnel by 4 magnets, 2 of them fit into the hollows in the support, while 2 fit on the outer side of the plexiglass (Fig. 10). Thanks to the consoles (Fig. 11) the models to

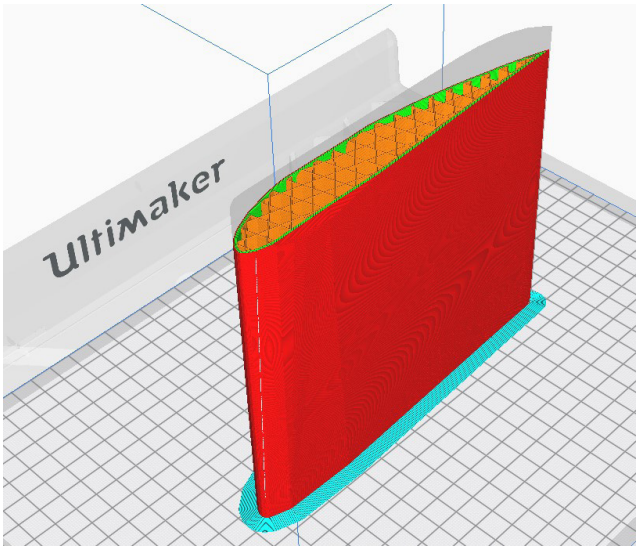

Fig. 9 3D print-ready CAD model

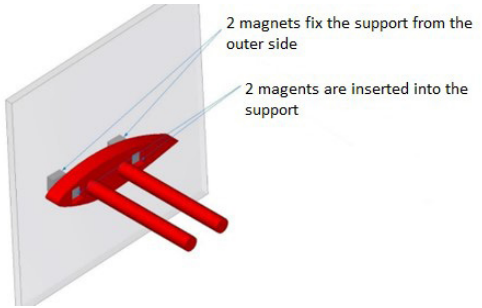

Fig. 10 Support fixed with magnets

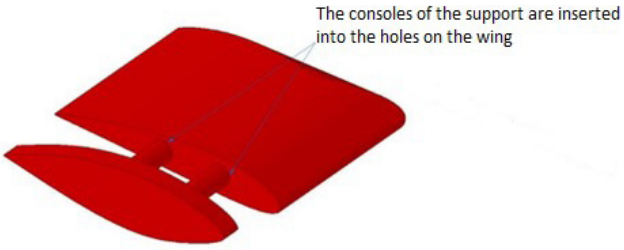

Fig. 11 The installation of the wing

be tested can be easily mounted to and removed from the wind tunnel (Fig. 12). After printing, the model can be examined in the wind tunnel (Fig. 13).

By moving the external magnets, the wing profile can be easily adjusted to any position, because thanks to the fixing technology, the model in the wind tunnel will follow the movement of the external magnets. Thus, the model can be moved freely in the vertical and horizontal directions, as well as rotated around its own axis, thereby setting any desired angle of incidence.

2.1.3 Results of wind tunnel examination

The tests are performed with a Clark Y profile wing design without any kind of wingtip device. After printing, the profile can be placed in the experimental space of the wind tunnel using the universal support. Flow around the wing is made to be visual with the help of smoke produced by a glycerin fog machine, as shown in Fig. 13. A digital anemometer can be used to measure the flow speed in the tunnel. A flow speed of 2 m/s can be achieved in the case of fans being operated at maximum power. Although this is well below the cruising speed of airplanes, it was confirmed during tests with smoke that vortices can form behind the wingtips even under such conditions. This can be seen in Fig. 14. The contour of the vortex cannot be determined clearly, since it is a local change in air pressure in a space that can be considered infinite, therefore the degree of swirling cannot be verified by calculation (Houghton et al., 2017), it can only be examined visually.

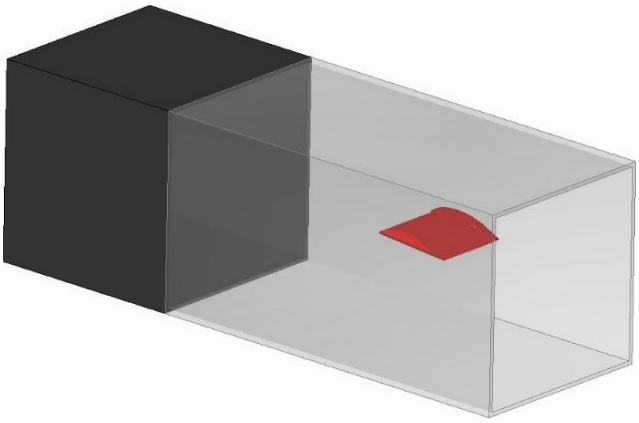

Fig. 12 Wing profile installed in the wind tunnel

Fig. 13 3D printed model in the wind tunnel

2.2 CFD simulations

Based on the mentioned aspects in Section 3, with the help of additive manufacturing, we can easily produce models for wind tunnel tests, however, the disadvantages of these tests are that the available speed range is very small, measurements in the wind tunnel are difficult, and the occurrence of measurement errors is high. In order to avoid these errors, it is worth carrying out the further tests with the help of computer simulation, however, before starting them, the accuracy and realism of the computer simulation need to be examined.

2.2.1 Modeling the wing profile

The tested Clark Y profile can be downloaded from the online model library (Fig. 15). The surface roughness specific for FDM printed parts is around Ra12.5 (Pérez et al., 2018). This must be set for the CAD model to get accurate and realistic results from the simulation.

2.2.2 CFD simulations with FloEFD

The flow studies of the model can be performed with the FloEFD (version 2020.2) extension of Solid Edge.

Fig. 14 The vortex is made visible with smoke

Fig. 15 CAD model ready for CFD simulations

For aerodynamic examinations, it is necessary to set the appropriate parameters in the program, which in our case are the same as those used and measured in the wind tunnel. These conditions are listed in Table 1.

After completing the preliminary settings, the program creates a virtual, finite space and places the model in it. The simulation will be run in this space, and the program will create a virtual mesh here. Therefore, it is advisable to set this space to the same size as the experimental space of the wind tunnel (length: 500 mm, cross-section: 250 × 250 mm). The virtual space and the model is shown in Fig. 16.

The FloEFD uses a Cartesian mesh to create the flow around the body to be examined, so in order to achieve good results, it is necessary to properly manage the mesh settings. During meshing, mesh refinement is created by the cell mating technique. It divides the starting base mesh (marked in blue in Fig. 17) into additional elements by side splitting, creating refinement level 1 (turquoise). If necessary, the mesh can be further thickened up to refinement level 7 with additional side halving. During a mesh refinement, element splitting occurs along the X, Y and Z axes

Table 1 Conditions set for the measurement

	Value	Unit
Flow speed	2	m/s
Air pressure	101,325	Pa
Temperature	293.2	K
Angle of incidence	10	°

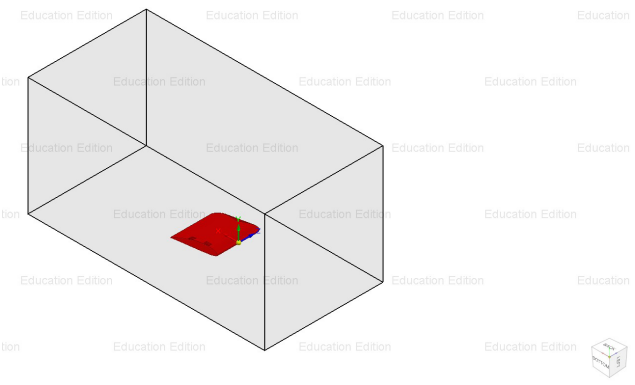

Fig. 16 Virtual space for the simulation

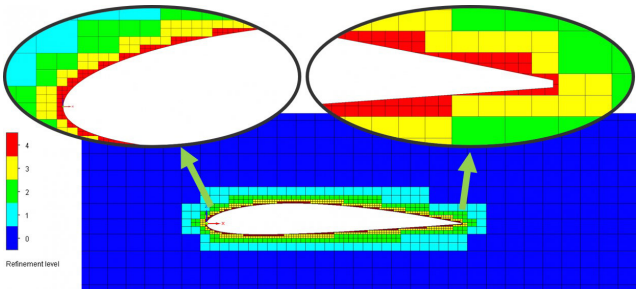

Fig. 17 Refinement level

of the element, therefore one element always becomes eight new elements (Hetyei, 2021).

The FloEFD offers two mesh refinement methods. One is local and the other is global refinement. On the local refinement, a specific surface can be selected on which we want to carry out the test, while global refinement creates the mesh for the entire volume of the previously set experimental space. In the investigation, we would like to examine first the updraft created at the wingtip and the vortices created behind it, so it is advisable to choose the global mesh. For this study, medium dense mesh is used, which is dense enough to adequately model the relatively low-velocity flow, but can be run in a significantly faster time than a higher refinement, therefore more simulations can be performed in a short time.

After completing all the necessary settings, the simulation can be run, after which we will have the opportunity to perform various examinations. In our case, the simulation divides the experimental area into 251,615 cells.

Since the default settings of FloEFD has been used for the simulation, the turbulence model was k-epsilon, while the wall treatment method was two-scale wall functions model. In the moment of measurements the time domain was in steady-state.

2.2.3 The results of CFD simulation

After running the simulation, the flow of the medium can be visualized.

As shown in Fig. 18, the vortex behind the wing can be clearly observed, similar to that experienced during wind tunnel tests.

If we examine the flow from the other direction as well (Fig. 19), we can observe the updraft created on the wingtip, as described in Section 2.2.

In Fig. 19, the flow at an increased speed on the upper and front part of the wing, which causes the pressure difference necessary for the development of lift force, can be clearly observed. Flow speed increases to 2.5 m/s on this

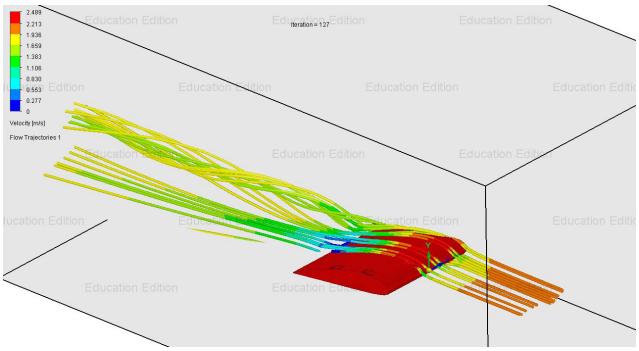

Fig. 18 Observable vortex in the CFD simulation

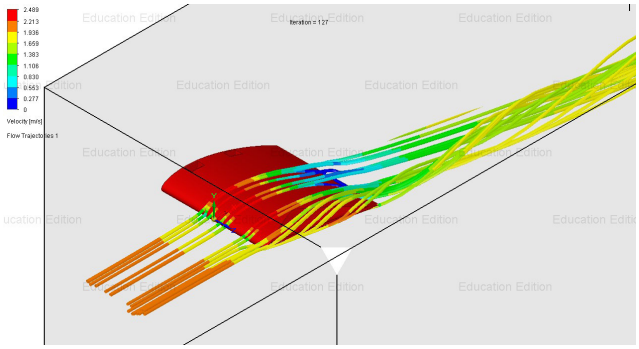

Fig. 19 Updraft on the wingtip

area, therefore. The resulting pressure drop in the upper part of the wing can be seen in Fig. 20.

Fig. 20 also shows an area on the top section of the wing, where the flow velocity slows down very much, almost to zero. This occurs due to the flow velocity being very low, the streamlines are no longer able to follow the curvature of the wing and separate from the wing at a certain point.

During flight, a laminar flow is experienced around the wing, however, as the speed decreases, a speed is reached at which the above-mentioned phenomenon occurs, and a turbulent flow develops on the top section of the wing, which can be observed in Fig. 21. This is the so-called stall speed (Szirtes and Rózsa, 2007) at and below which the lift is not enough to keep the airplane in the air.

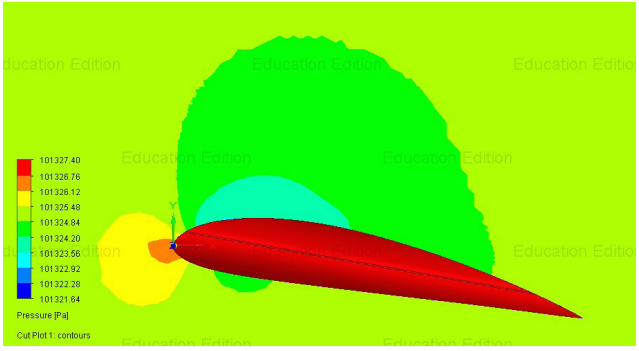

Fig. 20 Air pressure around the wing

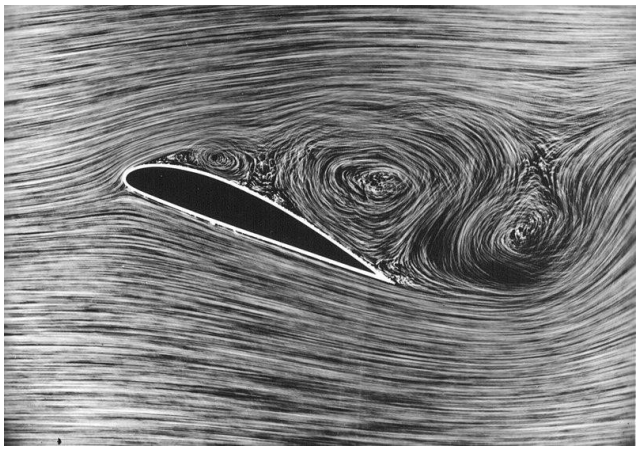

Fig. 21 Airflow at stall speed

3 Comparison of the wind tunnel and CFD tests

Based on the above discussed, it can be concluded that the simulations performed with the FloEFD program produce similar results to those that occur in reality, however, in order to draw a more accurate conclusion, it is necessary to compare the obtained results with those experienced during the physical wind tunnel simulations. For comparability, it is necessary to set the same conditions for the wind tunnel simulation and for computer simulation. Thus, in both cases, the angle of incidence is 10 degrees, the flow velocity of the medium is 2 m/s, and the ambient pressure and temperature are 101,325 Pa and 20 °C.

The two results can be easily compared by putting the image of the wind tunnel flow visualized with smoke next to the image of the computer simulation (Fig. 22). Since the contours of the vortex cannot be clearly determined, the result cannot be verified by calculation, only by visual

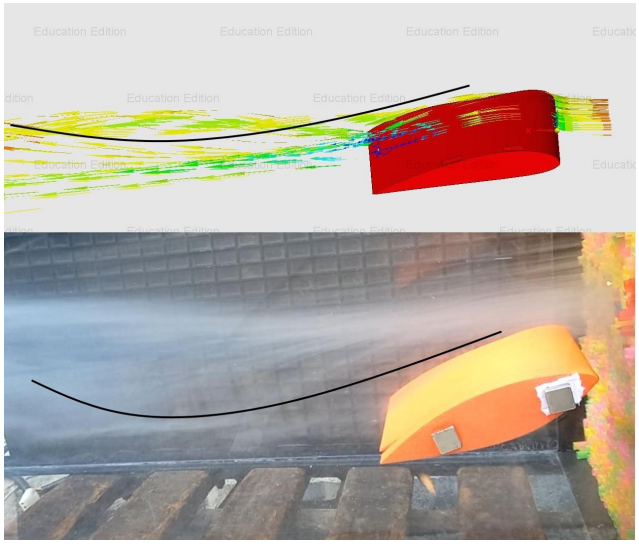

Fig. 22 CFD vs. wind tunnel simulation

methods. Thus, if we manage to find the same streamline in both cases, we can establish the identity by comparing them.

Since the two streamlines can be considered almost identical, it can be concluded that FloEFD is able to create simulations similar to the real world. At the same time, the wind tunnel is not suitable for effective experiments due to the low speed available in it and the measurement difficulties, so the use of computer simulation is justified in future tests in order to examine the effectiveness of the wingtip devices. With the help of computer simulations any number of wingtip designs can be tested quickly and easily. The design that seems to be the best based on CFD simulations must of course be printed and its suitability must be verified in the wind tunnel.

It is important to note that numerical flow simulations have many pitfalls and sensitive points. Therefore, it is necessary to validate the results obtained during the simulations (Hetyei et al., 2020).

4 Analysis

After eliminating the testing difficulties, caused by the ineffective wind tunnel tests, it is necessary to test different types of wingtips in order to prove which one works the most efficiently and which one can achieve the greatest aerodynamic drag reduction. This can also be calculated numerically in FloEFD.

In order to eliminate the stall speed mentioned in Section 4.3, this time the tests are carried out with a flow speed of 20 m/s (Table 2). The CAD models used in the CFD simulations are designed with reverse engineering based on existing wingtip devices.

4.1 Wing without wingtip device

In reality, no airplane wing has the design shown in Fig. 23, but in the goal of comparison, this type needs to be examined as well.

Table 3 illustrates the results of the CFD simulation where x is the axis parallel with the flow direction and y is the axis perpendicular to the flow direction. Compared to the size and weight of the examined model, the values obtained are realistic for F_x = 0.058 N and F_y = 0.74 N.

Table 2 Parameters set for the CFD simulation

	Value	Unit
Flow speed	20	m/s
Air pressure	101,325	Pa
Temperature	293.2	K
Angle of incidence	0	°

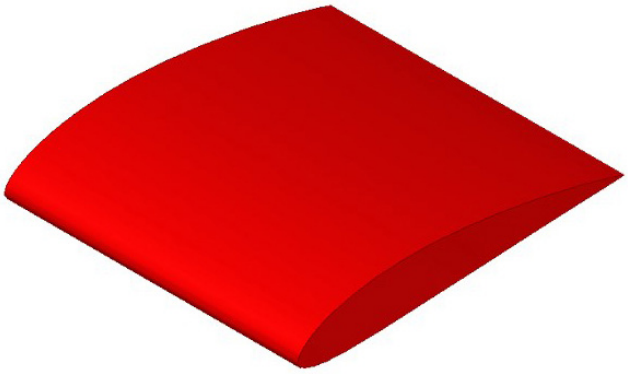

Fig. 23 Wing with no wingtip device

Table 3 Measurement results (no wingtip device)

Force	Value	Unit
F_x	0.058	N
F_y	0.74	N

With the help of these, the glide ratio or lift-to-drag ratio (MacEachern and Yıldız, 2018) can be easily calculated, which can also be interpreted as an indicator of the aircraft's fuel efficiency.

$$\frac{F_y}{F_x} = \frac{0.74}{0.058} = 12.75:1 \tag{1}$$

4.2 Rounded wingtip

Nowadays, the design shown in Fig. 24 is not common anymore, as it is not very effective in terms of efficiency, but we can still find similar ones on older planes, for example on the Antonov An-2.

Table 4 shows the results of tests carried out with this wingtip design. F_x = 0.055 N and F_y = 0.76 N. It can be

Fig. 24 Rounded wingtip

Table 4 Measurement results (rounded wingtip)

Force	Value	Unit
F_x	0.055	N
F_y	0.76	N

observed that compared to the previously examined wing, the lift increases minimally, while the air resistance decreases minimally, so the glide ratio:

$$\frac{F_y}{F_x} = \frac{0.76}{0.055} = 13.81:1. \quad (2)$$

4.3 Winglet/Sharklet

Today's most common wingtip design, the CAD model of which is shown in Fig. 25. The introduction of the Sharklet began in the 1980s on the Airbus A320 family, and then the Winglet with similar geometric characteristics appeared on the B737NG family.

F_x = 0.05 N and F_y = 0.76 N. In this case, there was no significant change in lift force compared to the model with a rounded wingtip, but the drag was reduced.

$$\frac{F_y}{F_x} = \frac{0.76}{0.05} = 15.2:1 \quad (3)$$

By comparing the glide ratio obtained in the case of wings with wingtip device and wings with rounded tip, it can be determined which design proved to be more efficient:

$$\frac{15.2}{13.81} \times 100 = 110\%. \quad (4)$$

In the case of the analyzed profiles, the wing profile with Winglet/Sharklet has a 10% better glide ratio than the rounded wingtip. Since the glide ratio is directly proportional to the fuel consumption, it can be stated that the examined wingtip device really effectively contributes to the reduction of fuel consumption.

4.4 Split Winglet

From the tests shown above, we could see the positive effects of wingtip devices. However, it is worth investigating which of these has the best efficiency. According to Boeing, the Split Winglet used on the B737MAX family is the most efficient wingtip device ever installed on a commercial aircraft. Fig. 26 shows the CAD model of the split wingtip used for the simulations.

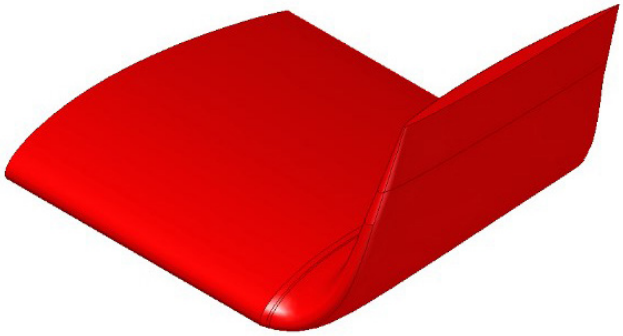

Fig. 25 Winglet/Sharklet

For the split winglet, the glide ratio can be calculated using the simulation results shown in Table 5.

$$\frac{F_y}{F_x} = \frac{0.762}{0.05} = 15.24:1 \quad (5)$$

If we compare the efficiency of the Winglet with the Split Winglet:

$$\frac{15.24}{15.2} \times 100 = 100.26\%. \quad (6)$$

4.5 Result examination

The measurement results obtained for the four examined profiles can be compared with the help of Table 6.

To sum up, the different wingtip designs have a significant influence on the glide ratio; even the simple, rounded wingtip achieved a better efficiency than the profile without wingtip device. However, by using wingtip devices, significant improvement can be achieved in the

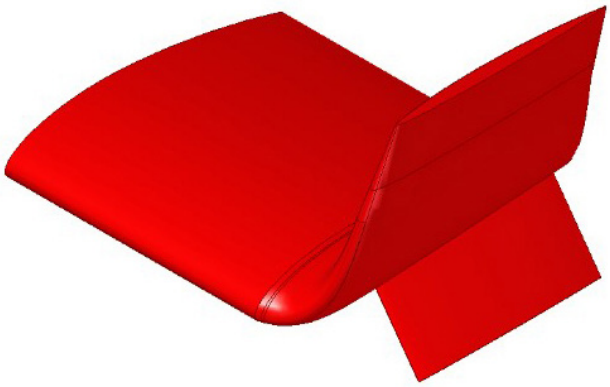

Fig. 26 Split Winglet

Table 5 Measurement results (Split Winglet)

Force	Value	Unit
F_x	0.050	N
F_y	0.762	N

Table 6 Comparison of the results

	F_y	F_x	Glide ratio	Efficiency
Unit	N	N	–	%
No wingtip	0.74	0.058	12.75 : 1	100
Rounded wingtip	0.76	0.055	13.81 : 1	108.3
Winglet/Sharklet	0.76	0.05	15.2 : 1	119.2
Split Winglet	0.762	0.05	15.24 : 1	119.5

Note: the efficiency values in the table shows the comparison of profiles with different wingtip designs to profiles with no wingtip.

lift-to-drag ratio, and therefore in fuel consumption as well. Furthermore, it can be observed that the efficiency difference among the specific Winglet and Sharklet designs is minimal, but even better results might be achieved by calibrating the geometrical characteristics.

5 Summary of the study

The goal of present research was to examine different types of wingtip devices in order to determine whether the use of wingtip devices really has a positive effect on the fuel consumption of airplanes, by evaluating the obtained measurement results.

Before starting the research, it was necessary to define the relationship between lift and aerodynamic drag, as well as the drag's negative effects on airplane wings. After the specification of the induced drag, it became necessary to choose the method to be used for the tests. The easiest way seemed to be carried out under real conditions, in a wind tunnel, with test specimens produced using additive manufacturing technology. However, due to the low performance of the wind tunnel and the measurement difficulties, it turned out that a more accurate solution had to be found. This is how the computer simulation was chosen, which could be done in Solid Edge with the help of the FloEFD addon. However, the effectiveness of this is questionable, so the measurement results need to be validated. Visual methods were used to examine the effectiveness of the computer simulation, which proved to be adequate.

After that, CFD tests for different wingtip devices could be started. As a result, it can be concluded that the glide ratio of the wings with Winglets is much better, thus the fuel consumption and CO_2 emissions of the aircraft will be lower.

As the continuation of this research, further tests will be necessary. The wing profile equipped with the Split Winglet – proved to have the best glide ratio – must be manufactured with 3D printing method in order to conduct wind tunnel tests to validate the CFD results. Simulations should also be performed at different angles and flow speeds.

References

Aghakhani, A., Takács, Á. (2023) "The meaning of concept in design methodology", Design of Machines and Structures, 13(1), pp. 5–11. https://doi.org/10.32972/dms.2023.001

David, A. (2024) "Sustainable freight forwarding – inland navigation", Cognitive Sustainability, 3(1). https://doi.org/10.55343/cogsust.101

Dömötör, C. (2023) "Reconstruction of Simple Parts Using FDM Technology", Design of Machines and Structures, 13(2), pp. 13–21. https://doi.org/10.32972/dms.2023.013

Dul, S., Gutierrez, B. J. A., Pegoretti, A., Alvarez-Quintana, J., Fambri, L. (2022) "3D printing of ABS Nanocomposites. Comparison of processing and effects of multi-wall and single-wall carbon nanotubes on thermal, mechanical and electrical properties", Journal of Materials Science & Technology, 121, pp. 52–66. https://doi.org/10.1016/j.jmst.2021.11.064

Espinoza-Fraire, A. T., López, A. E. D., Morado, R. P. P., Esqueda, J. A. S. (2023) "2 - Aerodynamic principles", In: Design of Control Laws and State Observers for Fixed-Wing UAVs: Simulation and Experimental Approaches, Elsevier, pp. 7–18. ISBN 978-0-323-95405-1 https://doi.org/10.1016/B978-0-32-395405-1.00011-X

Gudmundsson, S. (2022) "Chapter 16 - Aircraft Drag Analysis", In: General Aviation Aircraft Design: Applied Methods and Procedures, Butterworth-Heinemann, pp. 657–752. ISBN 978-0-12-818465-3 https://doi.org/10.1016/B978-0-12-818465-3.00016-1

Hallion, R. P. (2021) "The History of Air Transportation", In: Vickerman, R. (ed.) International Encyclopedia of Transportation, Elsevier, pp. 192–197. ISBN 978-0-08-102672-4 https://doi.org/10.1016/B978-0-08-102671-7.10425-7

Hetyei, C. (2021) "Kellően sűrű a hálóm? IV. – Lokális hálósűrítés FLOEFD-n belül" (Is the mesh dense enough? IV. – Local mesh compaction within FLOEFD), EPLM Blog, Nov. 03. [online] Available at: https://blog.eplm.hu/kelloen-suru-a-halom-iv-lokalis-halosurites-floefd-n-belul/ [Accessed: 29 April 2024] (in Hungarian)

Hetyei, C., Molnár, I., Szlivka, F. (2020) "Comparing different CFD software with NACA 2412 airfoil", Progress in Agricultural Engineering Sciences, 16(1), pp. 25–40. https://doi.org/10.1556/446.2020.00004

Houghton, E. L., Carpenter P. W., Collicott, S. H., Valentine, D. T. (2017) "Chapter 7 - Wing Theory", In: Aerodynamics for Engineering Students, Butterworth-Heinemann, pp. 449–523. ISBN 978-0-08-100194-3 https://doi.org/10.1016/B978-0-08-100194-3.00007-9

Kónya, G., Ficzere, P. (2024) "The Effect of Layer Thickness and Orientation of 3D Printed Workpieces, on The Micro- and Macrogeometric properties of Turned Parts", Acta Polytechnica Hungarica, 21(2), pp. 231–250.

MacEachern, C., Yıldız, I. (2018) "1.16 Wind Energy", In: Dincer, I. (ed.) Comprehensive Energy Systems, Elsevier, pp. 665–701. ISBN 978-0-12-814925-6 https://doi.org/10.1016/B978-0-12-809597-3.00118-8

Pérez, M., Medina-Sánchez, G., García-Collado, A., Gupta, M., Carou, D. (2018) "Surface Quality Enhancement of Fused Deposition Modeling (FDM) Printed Samples Based on the Selection of Critical Printing Parameters", Materials, 11(8), 1382. https://doi.org/10.3390/ma11081382

Restás, Á. (2013) "Az UAV közszolgálati alkalmazásai" (Public service applications of UAV), In: Palik, M. (ed.) Pilóta nélküli repülés profiknak és amatőröknek, Nemzeti Közszolgálati Egyetem, pp. 241–280. ISBN 978-615-5057-64-9 (in Hungarian)

Schröder, D., Leweke, T., Hörnschemeyer, R., Stumpf, E. (2022) "Generation of a wingtip vortex pair using a pressure-side fin", Aerospace Science and Technology, 130, 107860. https://doi.org/10.1016/j.ast.2022.107860

Siemens "FloEFD (version 2020.2)", [computer program] Available at: https://plm.sw.siemens.com/en-US/simcenter/fluids-thermal-simulation/floefd/ [Accessed: 01 September 2023]

Sy, M. S., Abuan, B. E., Danao, L. A. M. (2020) "Aerodynamic Investigation of a Horizontal Axis Wind Turbine with Split Winglet Using Computational Fluid Dynamics", Energies, 13(18), 4983. https://doi.org/10.3390/en13184983

Szirtes, T., Rózsa, P. (2007) "CHAPTER 18 - Fifty-two additional applications", In: Applied Dimensional Analysis and Modeling, Butterworth-Heinemann, pp. 527–657. ISBN 978-0-12-370620-1 https://doi.org/10.1016/B978-012370620-1.50024-1

Timmons, D., Terwel, R. (2022) "Economics of aviation fuel decarbonization: A preliminary assessment", Journal of Cleaner Production, 369, 133097. https://doi.org/10.1016/j.jclepro.2022.133097